Chapter 8
Nanowire-Enabled Energy Storage

Abstract A variety of energy storage systems are currently being explored and in some cases commercialized to meet the needs for both small and large-scale energy storage/usage. Among these systems, rechargeable batteries have been extensively investigated in the research community in efforts to make breakthroughs beyond existing commercial lithium ion systems and thereby provide enhancements to capacity, power density and other metrics that would be beneficial to ubiquitous consumer electronic devices through electric automobiles. In this chapter, the advantages of NW structures for efficient energy storage will be illustrated and discussed, including their high surface area, efficient charge transport and capability to sustain large volume expansion/contraction during charge/discharge cycles. In particular, we will introduce and discuss representative works focused on lithium ion batteries, electrochemical capacitors, and sodium ion batteries. Finally, prospects and challenges for implementing NWs for practical energy storage solutions will be briefly discussed.

8.1 Introduction

A significant challenge of this century centers on energy, and in particular, how can clean and renewable energy be efficiently produced as well as stored for efficient reuse and/or distribution [1–5]. In the case of energy storage, the performance, for example of batteries, depends intimately on the properties of anode and cathode materials. Innovative nanomaterials chemistry lies at the heart of advances that have already been made in improving rechargeable lithium–ion batteries (LIBs) [6, 7]. Further breakthroughs in materials can further fuel improvements of existing storage systems and also hold the key to new generations of energy storage devices. In this regard, nanostructured materials have attracted great interest in recent years because of the unusual mechanical and electrical properties endowed by confining the dimensions of such materials, and because the combination of bulk and high surface area properties can further enhance overall behavior. For example, battery electrode materials that in bulk form would degrade or fail due to large volume

A. Zhang et al., *Nanowires*, NanoScience and Technology,
DOI 10.1007/978-3-319-41981-7_8

changes during charge/discharge cycles can become viable in nanoscale morphologies, since the latter are capable of sustaining much greater strains before failure.

In this context, NWs are becoming increasingly important for electrochemical energy storage, and they represent unique candidates with several exciting advantages [8, 9]. First, the direct attachment and electrical contact of each NW to the metallic current collector provide efficient, 1D charge transport pathways, without the need of adding binders and conducting additives. Second, the void space between adjacent NWs and the high surface-to-volume ratios of NWs allow for fast penetration of electrolyte solution into deep portion of NWs, as well as rapid electrochemical reactions over the surface. Third, compared to flat electrode structures, the small diameters and the large curvatures of NWs are beneficial for accommodating more volume change, thus reducing mechanical failure of electrodes and maintaining the electronic pathways during many discharge-recharge cycles. In this chapter, we will introduce and discuss representative NW studies focused on lithium ion batteries (LIBs), electrochemical capacitors (ECs), and sodium ion batteries.

8.2 Lithium–Ion Batteries

Rechargeable LIBs are efficient, light-weight, and rechargeable power sources for a large variety of applications ranging from portable electronics to the development of electric automobiles, in which the electrodes are the central issue [10, 11]. A combination of a negative lithium intercalation material (anode) with another lithium intercalation material (cathode) having a more positive redox potential gives a Li–ion transfer cell [12]. An anode and a cathode are separated by an electrolyte, which is an electronic insulator but a Li–ion conductor. Upon charging, lithium ions are released by the cathode and intercalated at the anode. When the cell is discharged, lithium ions are extracted by the cathode from the anode. An ideal electrode should provide high gravimetric and volumetric capacity, high power density and long cycle life, as well as being environmentally benign and low cost [13]. One of the main challenges in the design of LIBs is to ensure that the electrodes maintain their integrity over many discharge-recharge cycles. Although promising electrode systems have been proposed, their lifespans are often limited by Li–alloying agglomeration or the growth of passivation layers, which prevent the fully reversible insertion of Li ions into the negative electrodes (anodes) [14]. 1D NWs, especially the self-supporting NW arrays grown directly on a current-collecting substrate offer several attractive features for LIB electrodes [15]. The open space between neighboring NWs allows for easy diffusion of electrolyte into the inner region of the electrode, resulting in reduced internal resistance and improved high-power performance. Each NW has its own contact with the current collector substrate, which can ensure that every NW participates in the electrochemical reaction. In addition, using NW arrays also saves the tedious process of mixing

active material with ancillary materials such as carbon black and polymer. Moreover, NWs share the same advantages as other nanostructured electrodes, such as nanoparticles, with high electrode-electrolyte contact area, fast Li–ion diffusion rate, and good strain accommodation.

8.2.1 Anodes

8.2.1.1 Si

Si has the highest gravimetric capacity (4200 mAh/g, lithiated to $Li_{4.4}Si$) among all anode candidates other than Li metal [10]. The average discharge voltage of Si is low (~0.4 V), providing a high voltage difference against the cathode [16]. Nonetheless, the insertion and extraction of lithium ions from Si leads to a large volume change, up to ~400 % volume increase upon insertion, and this large volume change results in mechanical failure of electrodes and discontinuous charge transport during cycling (top, Fig. 8.1a). In addition, the large volume change also affects the formation of dense and stable solid-electrolyte inter-phase (SEI) layer over Si surface, which functions as an ionic conducting and electronic insulating passivation layer to prevent further side chemical reactions from occurring [13]. Thus, the Si-based anode usually suffers from substantially reduced stability and a large irreversible capacity decrease during charge/discharge cycles [17].

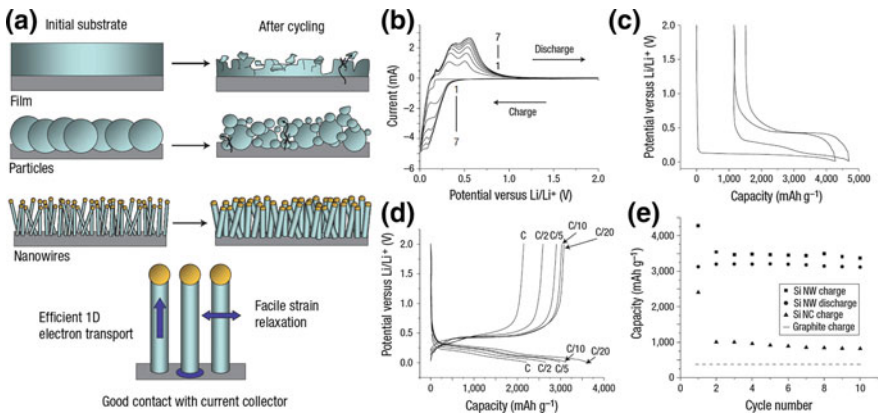

Fig. 8.1 **a** Schematics of the morphological changes that occur in Si during electrochemical cycling, where Si films and particles tend to fail during cycling, while NWs grown directly on the current collector do not break-up into smaller particles. **b** Cyclic voltammograms for SiNWs from 2.0 to 0.01 V versus Li/Li^+. The first seven cycles are shown. **c** Voltage profiles for the first and second galvanostatic cycles of the SiNWs. The first charge achieved the theoretical capacity of 4200 mAh g^{-1} for $Li_{4.4}Si$. **d** The voltage profiles for the SiNWs cycled at different power rates. **e** Capacity versus cycle number for the SiNWs at the C/20 rate showing the charge (*squares*) and discharge capacity (*circles*). The charge data for Si nanocrystals (*triangles*) and the theoretical capacity for lithiated graphite (*dashed line*) are shown as a comparison to show the improvement when using SiNWs. Reproduced from [8]. Copyright 2008 Nature Publishing Group

A number of research efforts have addressed these challenges of Si anodes for LIBs by focusing on the rational design and fabrication of Si-based nanostructures [18–20]. In 2008, the Cui group [8] reported the first SiNW-based LIB anode, in which SiNWs were grown by the nanocluster-catalyzed VLS method on stainless steel substrates (Fig. 8.1a). LIB anodes made using these SiNW electrodes achieve nearly the theoretical discharge capacity of Si during the first cycle, and maintained a discharge capacity of ~3100 mAh/g, about 75 % of the maximum, with little fading over 10 cycles (Fig. 8.1b–e). Structural characterization after the battery test showed an increase of SiNW diameter from 89 nm initially to 141 nm after lithiation, and importantly, demonstrated that the SiNWs remained connected with the current collectors versus breaking up into smaller particles. These latter results suggested that the nanoscale diameters provided superior mechanical properties and allowed the SiNWs to sustain the strains associated with large volume changes during charge/discharge cycles.

Similar to VLS-grown samples, SiNWs made by other approaches have been investigated as LIB anode materials. For example, Schulz et al. [21] reported using an electrospinning method with Si_6H_{12} as the Si precursor to synthesize Si nanofibers, while the LIB anodes made of these samples only achieve a reversible capacity ~400 mAh/g after 30 cycles. On the other hand, SiNWs fabricated by the metal-assisted solution etching approach have exhibited characteristics similar to nanocluster-catalyzed VLS NWs, and thus are good candidates for LIB anodes. An added advantage of this latter etching-based approach to SiNWs is that it is possible to precisely control the crystal orientation and doping based on the starting Si-substrate [18, 22, 23]. The rougher surface of solution etched SiNWs also increases the surface area, which could be beneficial for the insertion/extraction of Li ions [18]. As a result, SiNWs obtained from the solution etching approach have demonstrated substantially improved capacity and cycling stability for the use of LIB anodes [24, 25].

SiNWs with core-shell designs provide additional structural advantages in optimizing the electrochemical performance for Si-based anodes. For example, a thin carbon shell could facilitate electrical contact and charge conduction. Huang et al. [26] reported synthesis of carbon-coated etched SiNW arrays by pyrolysis of a carbon aerogel. Compared to the pristine SiNWs, which exhibited capacity fading after 10 cycles, the carbon-coated SiNWs showed a high initial discharge capacity of 3344 mAh/g and retained a reversible capacity of 1326 mAh/g after 40 cycles. The continuous structure of most of these SiNWs is still maintained after the cycling test. Polymer has also been demonstrated for coating of SiNWs for improving the stability and capacity of the anodes [27]. In addition, a scalable supercritical fluid-liquid-solid method was reported to grow SiNWs [28], which were further coated with carbon by pyrolysis of sucrose on the SiNW surface. LIB anodes made of these carbon-coated SiNWs have retained a reversible capacity of 1500 mAh/g after 30 cycles.

In addition to Si/carbon core/shell designs, Cui and coworkers has demonstrated the utilization of crystalline/amorphous core/shell SiNWs for enhanced lithium ion storage capacity [29]. The crystalline Si core and amorphous Si shell are sequentially grown via the nanocluster-catalyzed VLS and shell deposition strategies described in earlier chapters. As the amorphous Si shell reacts with Li^+ at a slightly higher potential than the crystalline Si core, this design of crystalline/amorphous core/shell SiNWs allows for selective lithiation of the amorphous Si shell. The crystalline Si core is not affected during the lithiation step and serves as a continuous structure for both electrical conduction and mechanical support, thus resulting in substantial improvement in power rate and cycling stability. Specifically, crystalline/amorphous core/shell SiNWs have demonstrated a reversible capacity of 1000 mAh/g over 100 cycles. TEM images revealed that the crystalline/amorphous core/shell SiNWs become completely amorphous when the anodes are discharged to 10 mV, while the crystalline Si core is maintained for discharge potentials above 150 mV. This structural characterization confirms that the enhanced stability is due to the existence of crystalline Si core after cycling.

This crystalline core/amorphous shell concept was further extended to the synthesis of carbon/Si core/shell NWs, in which amorphous Si layer is deposited on the surface of carbon nanofibers [30]. In this case, the carbon nanofiber core serves as an electrical conductor and stable mechanical support [31]. In addition, the carbon cores have much less volume change than that of Si, and thus the core structures are maintained at a much lower low discharge potential of $\sim$10 mV. A higher charge capacity of 2000 mAh/g was reported for carbon/Si core/shell NWs. In addition, other core/shell NW designs have been reported for amorphous Si on different core materials, including metal silicides [32], nitrides [33], and carbon nanotubes [34].

The shape and volume changes of crystalline SiNWs with different crystal orientations have been studied by in situ electron microscopy [35, 36]. SEM images showed that lithiation transforms the initially circular cross sections of NWs with $\langle 100 \rangle$, $\langle 110 \rangle$, and $\langle 111 \rangle$ axial orientations into expanded structures with cross sections having cross, ellipse, and hexagonal shapes, respectively [37] (Fig. 8.2a). These observations were explained in terms of a rapid lithium ion diffusion channel along the $\langle 110 \rangle$ direction, which causes preferential volume expansion along this direction. It was also found that the $\langle 111 \rangle$ and $\langle 100 \rangle$ NWs shrink in height after partial lithiation, while $\langle 110 \rangle$ NWs increase in height. This length contraction was attributed to a collapse of $\{111\}$ planes early in the lithiation process. In another work [38], the anisotropic swelling of SiNWs during lithiation in either a conventional liquid cell or an all-solid electrochemical cell was characterized by TEM (Fig. 8.2b). In this latter work, the authors directly observed that the large volumetric expansion $\langle 112 \rangle$ axis NWs occurs in a highly anisotropic fashion to yield intermediate dumbbell-shaped cross sections. These results give new insight into the Si volume change process and may help in designing better Si anodes.

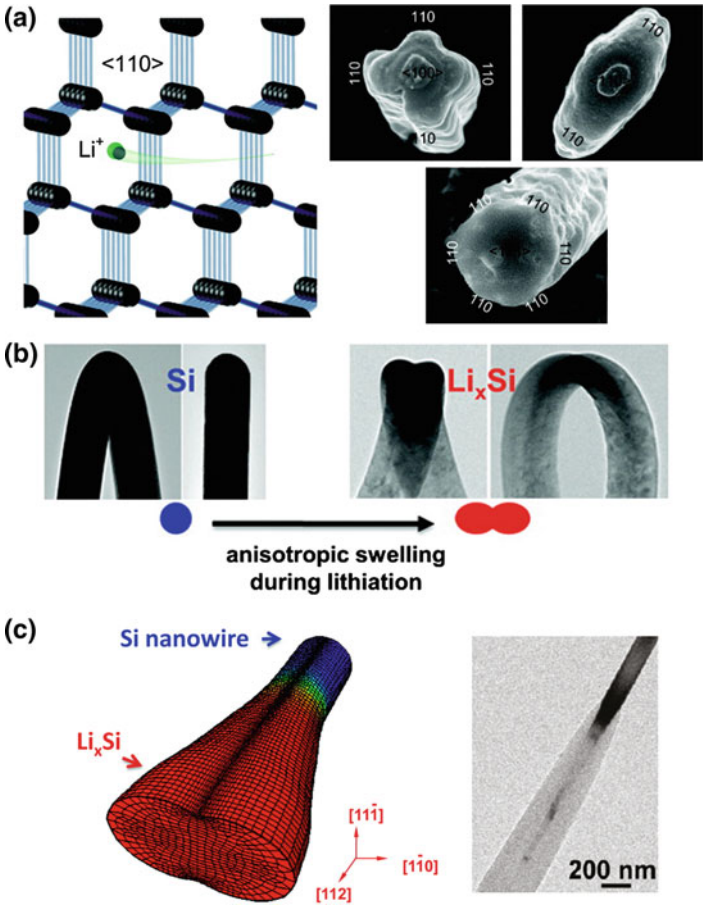

Fig. 8.2 **a** Anisotropic lateral expansion of crystalline SiNWs with ⟨100⟩, ⟨110⟩ and ⟨111⟩ axial orientations upon lithiation. Reproduced from [37]. Copyright 2011 American Chemical Society. **b** Dumbbell shape of a ⟨112⟩ axis SiNW following lithiation contrasts the round cross section of the pristine SiNW. **c** 3D simulation (*left*) and TEM image (*right*) of a progressively lithiated NW (i.e., the Li flux is prescribed at the front end), showing the development of the dumbbell-shaped cross section along the longitudinal direction. Reproduced from [38]. Copyright 2011 American Chemical Society

8.2.1.2 Metal Oxides

Metal oxides, especially in the form of nanomaterials, have been extensively investigated as potential anode materials for LIBs because these materials have diverse chemical and physical properties and most of them possess relatively high theoretical capacities between 500 and 1000 mAh/g compared to graphite (372 mAh/g) in commercial LIBs [39–42], although still much lower than the theoretical capacity of Si (4200 mAh/g) [10]. However, the use of metal oxides as LIB anodes still faces

multiple challenges including: (i) similar to Si, most metal oxides exhibit substantial expansion and contraction during charging/discharging processes [43, 44]; and (ii) most abundant metal oxides are semiconductors with large band gaps and typically have poor electrical conductivity and ion transport kinetics as LIB electrodes [41, 45]. To address these issues, researchers have been focused on the design of electrode structures and the use of multi-functional hybrid materials [39–42]. Based on the overall mechanism, metal oxide-based LIB anodes can be divided into three categories: (i) intercalation/deintercalation of Li ions into and from layered metal oxides; (ii) alloying/dealloying to store/release Li ions; (iii) conversion between Li and Li_2O by reduction/oxidation of transition metal oxides [39–42]. Here we focus on well-studied TiO_2, SnO_2 and Co_3O_4 NWs as examples for these three categories.

(i) Several transition metal oxides with layered and open channel structures can store Li ions via the intercalation/deintercalation mechanism [39–42]. These materials can exhibit a range of theoretical capacities depending on the structure of the metal oxide and number of Li ions intercalated into layer or channel sites during intercalation. This mechanism can be written as [39]:

$$MO_x + yLi^+ + ye^- \Leftrightarrow Li_yMO_x$$

For example, TiO_2, is a potential candidate for use as LIB anodes due to its low cost and abundance in nature, and has various polymorphs such as anatase, rutile, and TiO_2(B) (bronze). In 2005, the Bruce group [46] reported the intercalation of Li ions into TiO_2(B) NWs. TiO_2(B) NWs were synthesized by an ion-exchanging K^+ for H^+ in $K_2Ti_4O_9$ to form a hydrated hydrogen titanate, which was transformed into TiO_2 NWs by heating at 500 °C. The structure of TiO_2(B) NWs is composed of corrugated sheets of edge- and corner-sharing TiO_2 octahedra, with these sheets being linked together by bridging oxygen atoms to form a 3D network, with significant voids and continuous channels that are capable of rendering the material a host structure for intercalation. The reversible charge-storage capacity of 205 mAh/g was obtained without structural degradation or loss of NW morphology. In comparison, the capacity for bulk material is 240 mAh/g, with the composition $Li_{0.71}TiO_2$(B). The best result using other TiO_2(B) nanostructures was observed for needle-shaped TiO_2(B) nanoparticles with a reversible capacity of $\sim$288 mAh/g after 50 cycles [47].

(ii) Metal oxide anodes that undergo an alloying/dealloying mechanism typically have higher capacities than intercalation/deintercalation, but necessarily as a result of high capacity suffer from significant volume change during cycling [22]. The basic mechanism can be written in two steps [39]:

$$M_xO_y + 2yLi^+ + 2ye^- \Rightarrow xM + yLi_2O$$
$$M + zLi^+ + ze^- \Leftrightarrow Li_zM$$

Taking SnO_2 (theoretical capacity, 782 mAh/g) as an example, Park et al. [48] reported the preparation and electrochemical performance of SnO_2 NWs to determine their potential use as an anode material. The SnO_2 NWs were synthesized by thermal evaporation combined with a self-catalyzed growth procedure, where the authors used a high surface area powder to increase production at lower temperature. The SnO_2 NWs produced in this manner showed higher initial Coulombic efficiency and an improved capacity retention on cycling compared with those of SnO_2 powder and SnO_2 NWs produced by Au-assisted VLS growth. Kim et al. [49] reported the synthesis of SnO_2–In_2O_3 core-shell NW heterostructures via a thermal evaporation method. The electronic conductivity of the individual SnO_2–In_2O_3 core-shell NWs was 2 orders of magnitude higher than that of pure SnO_2 NWs, due to the formation of Sn-doped In_2O_3 during the nucleation and growth of the In_2O_3 shell nanostructures. Kim et al. [50] reported the synthesis of SnO_2 NWs using 1D mesoporous SiO_2 sacrificial templates that were subsequently dissolved in NaOH. These ultrasmall 6 nm diameter SnO_2 NWs with lengths >3 μm and surface area of 80 m^2/g exhibited a capacity of 800 mAh/g, while the capacity was reduced to 250 mAh/g at a 10C rate (4000 mA/g). Liu et al. [51] reported the synthesis of SnO_2 nanorod arrays on large-area flexible metallic substrates (Fe–Co–Ni alloy and Ni foil) via a hydrothermal process. The electrochemical behavior was found to depend crucially on the structural parameters of the array. An array consisting of SnO_2 nanorods of average 60 nm in diameter and 670 nm in length delivered a reversible Li-capacity as high as 580 mAh/g after 100 cycles (0.1C) and showed less than 50 % reduction to 350 mAh/g at a higher rate of 5C rate. Structural disintegration and agglomeration were not observed for the SnO_2 nanorod arrays even after 50 cycles. In comparison, commercially available ca. 40 nm SnO_2 particles yield an initial capacity of 500 mAh/g, although this capacity dropped to 100 mAh/g after 50 cycles [52]. The best performance so far was observed for 3 nm SnO_2 nanoparticles, which exhibited an initial capacity of 740 mAh/g with negligible capacity fading [53].

(iii) Li can be stored reversibly in transition metal oxides through a conversion reaction mechanism, where the transition metal experiences reduction/oxidation reactions [39–42] Anodes based on these materials also exhibits relatively high capacities (500–1000 mAh/g).

$$M_xO_y + 2yLi^+ + 2ye^- \Leftrightarrow xM + yLi_2O$$

For instance, the theoretical capacity of Co_3O_4 is 890 mAh/g. In 2008, Li et al. [15] utilized a mild template-free, ammonia-evaporation-induced method for large-area growth of self-supported Co_3O_4 NW arrays on different substrates, including Si wafers, glass slides, and Cu or Ti foils. Ti foil is an excellent substrate for this work, as it is resistive to the alkaline ammonia solution and oxidation, and it does not alloy with metallic Li at low voltage and thus serves as a good current collector. In addition, the NW arrays produced by their method had mesoporous

structures, which provided extra freedom for volumetric changes during lithiation. The NW arrays show a stable capacity of 700 mAh/g at 1C after 20 cycles, and can maintain the capacity around 50 % at a higher charging rate of 50C, substantially better than freestanding Co_3O_4 NWs not grown on Ti foils. Later, Wu et al. [54] reported a two-step hydrothermal synthesis of a Co_3O_4/α-Fe_2O_3 branched NW heterostructures. The single-crystalline, primary Co_3O_4 NW trunk arrays directly grown on Ti substrates allow for efficient electrical and ionic transport. The secondary α-Fe_2O_3 branches provide enhanced surface area and high theoretical Li^+ storage capacity, and can also serve as volume spacers between neighboring Co_3O_4 NW arrays to maintain electrolyte penetration as well as reduce the aggregation during Li^+ intercalation. These Co_3O_4/α-Fe_2O_3 branched NW heterostructures yielded improved electrochemical energy storage performance with reversible capacity of ∼980 mAh/g after 60 cycles. In comparison, the best performance using other nanomaterials so far was observed in graphene-encapsulated Co_3O_4 nanoparticles, exhibiting a reversible capacity of 1100 mAh/g in the first 10 cycles, and over 1000 mAh/g after 130 cycles [55].

8.2.2 Cathodes

Since the concept of a rechargeable lithium cell based on Li intercalation reactions was initiated in the early 1970s, numerous lithium intercalation cathode electrodes have been proposed to date [10]. Two categories of materials have been used for LIB cathodes [43, 56–58]. The first category include lithium transition metal oxides with layered anion close-packed lattice, where the transition metal ions occupy alternate layers and Li ions can be intercalated into the remaining layers. Commonly used materials include $LiCoO_2$, $LiNiO_2$ and $LiMn_2O_4$. One intrinsic advantage of this category of cathode is their higher energy density owning to their compact lattice structures. The second category includes layered materials with more open structures, such as V_2O_5 and transition metal phosphates (e.g., the olivine $LiFePO_4$). These materials provide the advantages of better safety and lower cost compared to the first category.

Currently, $LiCoO_2$, $LiNiO_2$ and $LiMn_2O_4$ are used as commercial LIB cathode materials, among which $LiCoO_2$ being the most popular candidate owing to the convenience and simplicity of preparation [10]. $LiCoO_2$ cathode materials are typically cycled with excellent stability between the fully lithiated discharge state $LiCoO_2$ (∼3.0 V vs. Li/Li^+) and a roughly half-delithiated state Li_xCoO_2 (x = 0.5–0.6, 4.2 V vs. Li/Li^+), leading to a capacity of ∼140 mAh/g, while its theoretical capacity is 273 mAh/g [59]. In 2005, Jiao et al. [60] reported a hard template route to synthesize $LiCoO_2$ NWs. Preliminary electrochemical tests using these $LiCoO_2$ NW arrays as cathodes showed an initial discharge capacity of 80 mAh/g and a capacity retention of 40 mAh/g after 50 cycles, much less than that of commercial $LiCoO_2$ cathodes [59]. Later, Xiao et al. [61] demonstrated the synthesis of cobalt precursor $Co(CO_3)_{0.35}Cl_{0.2}(OH)_{1.1}$ NW aggregates by a hydrothermal method, and

transformed these into Co_3O_4 NWs at high temperature. Subsequent reaction with LiOH yielded $LiCoO_2$ NWs. High-resolution TEM revealed that these $LiCoO_2$ NWs were composed of nanoparticles, with most of the nanoparticles having exposed (010) planes. The as-prepared $LiCoO_2$ NWs exhibited charge/discharge capacity stabilized at 100 mAh/g after 100 cycles. In comparison, the most recent report on flake-like $LiCoO_2$ nanoparticles synthesized using $Co(OH)_2$ nanoflakes as sacrificial templates via a simple coprecipitation method showed a reversible discharge capacity up to 179 mAh/g [62].

The disadvantages of $LiCoO_2$ as cathode material include its high cost and toxicity [43, 56–58]. As an alternative, $LiMn_2O_4$ can be a lower cost, environmentally friendly, and highly abundant material for LIB cathodes. The theoretical charge storage capacity is 148 mAh/g [63], although it can be limited due to phase changes during cycling [64, 65]. The Cui group [66] reported the hydrothermal synthesis of single-crystalline β-MnO_2 nanorods and their chemical conversion into free-standing single-crystalline $LiMn_2O_4$ nanorods. The $LiMn_2O_4$ nanorods had an average diameter of 130 nm and length of 1.2 μm. Galvanostatic battery testing showed that $LiMn_2O_4$ nanorods had a charge storage capacity of 100 mAh/g at a high current density of 148 mA/g (1C) with high reversibility and 85 % capacity retention after 100 cycles, while the capacity of commercially available powders was only 50 mAh/g at the same current density. Structural studies showed that the Li ions intercalated into the cubic phase of $LiMn_2O_4$ with a small change of lattice parameter, followed by the coexistence of two nearly identical cubic phases in the potential range of 3.5–4.3 V. Similarly, they also reported ultrathin $LiMn_2O_4$ NWs with cubic spinel structure synthesized by a solvothermal reaction. This approach produced α-MnO_2 NWs which were converted in a second step to $LiMn_2O_4$ NWs with diameters less than 10 nm and lengths of several micrometers [67]. These small diameters NWs yielded 100 and 78 mAh/g at high charging rates of 60 and 150C, respectively [67]. Hosono et al. [68] synthesized single crystalline cubic spinel $LiMn_2O_4$ NWs using $Na_{0.44}MnO_2$ NWs as a self-template. These self-templated NWs exhibited reversible capacities of 108, 102, and 88 mAh/g at fast charge/discharge rates of ~50, 100, and 200C, respectively. More recently, Wang et al. [69] reported an all NW based flexible LIB, using homologous Mn_2O_3 and $LiMn_2O_4$ NWs for anodes and cathodes, respectively. As shown in Fig. 8.3, the same precursors, MnOOH NWs, were transformed from hydrothermally grown MnO_2 nanoflakes and directly attached on Ti foils via reaction with poly(vinyl pyrrolidone). The Mn_2O_3 anode and $LiMn_2O_4$ cathode were subsequently formed by thermal annealing and reaction with lithium salt, respectively. The $LiMn_2O_4$ NW cathode showed a reversible capacity of 94.7 mAh/g at a charging rate of 1C and high capacity retention of ~96 % after 100 cycles. Furthermore, the flexible Mn_2O_3//$LiMn_2O_4$ full LIB exhibited an output voltage of >3 V, a thickness of 0.3 mm, high flexibility, and a specific capacity of 99 mAh/g based on the total weight of the cathode material. It also exhibited good cycling stability with a capacity of ~80 mAh/g after 40 charge/discharge cycles. Notably, a recent study reported the synthesis of nanoparticles with a new composition $Li_4Mn_2O_5$, prepared by direct mechanochemical synthesis at room temperature [70] yielded a discharge

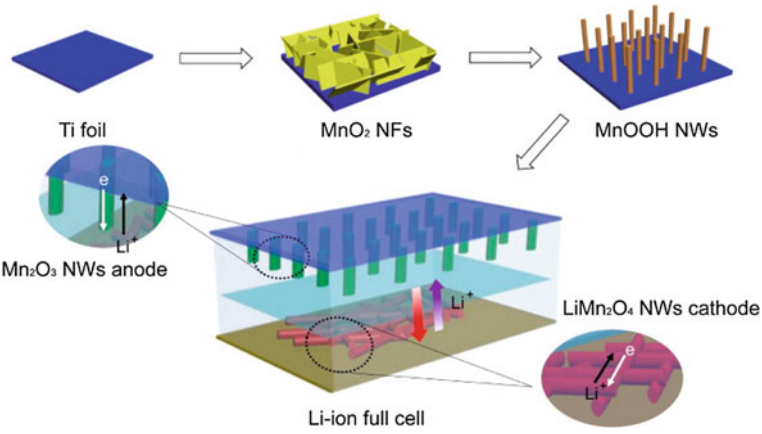

Fig. 8.3 Schematic of the synthesis and fabrication of the Mn_2O_3//$LiMn_2O_4$ LIB full cell. Reproduced from [69]. Copyright 2014 American Chemical Society

capacity of 355 mAh/g. This is the highest yet reported among known lithium manganese oxide electrode materials. Such a high capacity is in principle unexpected, as the oxidation state of Mn in $Li_4Mn_2O_5$ is 3+. If one assumes that only the Mn^{3+}/Mn^{4+} redox couple is active, then two Li ions could be extracted, resulting in the formation of $Li_2Mn_2O_5$ with a theoretical capacity of 245 mAh/g. According to the magnetic measurements, the authors proposed that the electrochemical activity is due to the Mn^{3+}/Mn^{4+}, O^{2-}/O^{-}, as well as Mn^{4+}/Mn^{5+} redox couples. Future studies could help to illuminate better these interesting results.

For Li ion intercalation applications, V_2O_5 offers advantages of low cost, natural abundance and straightforward synthesis [12]. Interestingly, different $Li_xV_2O_5$ phases form after intercalation of Li ions, each with different theoretical capacities. The highest capacity ω-$Li_xV_2O_5$ phase yields $\sim$440 mAh/g for deep discharge, although all of the intercalated Li ions cannot be extracted from the host structure, indicating an irreversible transition [71]. In 2010, Mai et al. [72] reported the synthesis of ultralong hierarchical V_2O_5 NWs with diameters of 100–200 nm and lengths up to several millimeters using electrospinning combined with annealing. As shown in Fig. 8.4, the hierarchical NWs were constructed from attached V_2O_5 nanorods of diameter $\sim$50 nm and length of 100 nm. The initial and 50th discharge capacities of the ultralong hierarchical V_2O_5 NW cathodes were 390 and 201 mAh/g when the LIB was cycled between 1.75 and 4.0 V, much higher than the self-aggregated short nanorods synthesized by a hydrothermal method. Chan et al. [73] used in situ TEM to study the chemical, structural, and electrical transformations of V_2O_5 nanoribbons at the single nanostructure level. It was found that transformation of V_2O_5 into the $Li_3V_2O_5$ phase depends not only on the width but also the thickness of the nanoribbons. Transformation can take place within 10 s in thin nanoribbons, suggesting a Li^+ diffusion constant that is 3 orders of magnitude faster than in bulk materials, resulting in a significant increase in battery

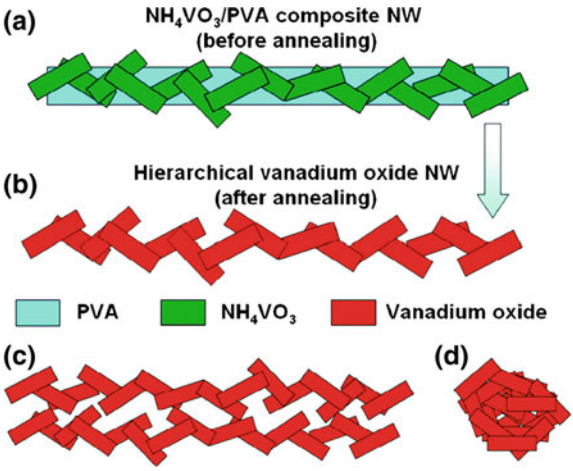

Fig. 8.4 **a**, **b** Schematic illustration of formation of the ultralong hierarchical vanadium oxide NWs during annealing. **c** Side view of two ultralong hierarchical vanadium oxide NWs near each other. **d** Self-aggregation of short vanadium oxide nanorods. Reproduced from [72]. Copyright 2010 American Chemical Society

power density. Recently, it was reported that NWs/nanorods assembled into a 3D interconnected V_2O_5 nano-network yielded improved electron/ion transport and enhanced structure stability [74]. The inner porous structure was proposed to promote ion diffusion and to buffer volume change during cycling. As a cathode, the interconnected V_2O_5 nano-network exhibited little capacity fading after 1000 charge/discharge cycles at high current densities of 1.0 and 2.0 A/g.

Lithium metal phosphates are presently at the center of much interest as cathodes for LIBs, with a theoretical capacity of 170 mAh/g for the commonly investigated $LiFePO_4$. Lim et al. [75] used a hard template for the synthesis of $LiFePO_4$ NWs. In this work, a 2D hexagonal Santa Barbara amorphous (SBA-15) silica template, containing parallel cylindrical pores arranged with a hexagonal *P6mm* symmetry, served to organize the wires into parallel bundles. After impregnation of the template with a solution consisting of $LiFePO_4$ precursor, the silica template was removed and the resultant $LiFeO_4$ NWs were subsequently annealed. Electrochemical cycling demonstrates the discharge capacity at a rate of 15C shows 137 mAh/g, corresponding to a capacity retention of 89 % compared with the capacity at a rate of 0.2C. This capacity value was less than that reported for hollow $LiFePO_4$ nanoparticles, which was 153 mAh/g at 15C and had a 95 % capacity retention compared to that at 0.2C.

8.3 Electrochemical Capacitors

LIBs are attractive energy storage devices in terms of their overall energy density (Wh/kg), although the rate of discharge and charge, which is defined by the power density (kW/kg), can be too slow for some applications [10, 11]. High power density needs can in principle be met by ECs, also known as supercapacitors or

ultracapacitors [76, 77]. ECs are power devices that can be fully charged or discharged in seconds, and can yield high power densities of the order of 10 kW/kg for short times [78]. There are two classes of ECs depending on the charge storage mechanism [41, 77, 79–81]. The first class is electrical double layer capacitors (EDLCs), which operate by adsorbing/desorbing charged ions from an electrolyte onto high surface area electrodes forming a double layer structure. Carbon-based materials with high surface area are typically used for EDLCs. A second group of ECs, known as pseudo-capacitors or redox supercapacitors, use transition metal oxides or conducting polymers as electrode materials, with the charge storage depending on fast Faradaic redox reactions. Energy and power densities are two crucial parameters for evaluating the EC performance. The maximum energy, E, and power densities, P, of a EC can be obtained using the following equations [78]:

$$E = CV^2/2$$
$$P = V^2/4R$$

where C is the specific capacitance (SC) of the cell, V is the operating voltage, and R is the series resistance. Therefore, a good EC should possess a high SC, wide operating voltage, and minimum resistance. The advantages of nanomaterials in ECs include: (i) the large surface to volume ratio, which provides more ion adsorption or active sites for the formation of electrical double-layer and charge-transfer reactions; (ii) short diffusion and transport length scales for electrolyte ions within the nanostructures, which can facilitate transport of electrolyte ions; and (iii) can effectively buffer stress from volume change in redox EC electrodes during charge/discharge. In this section, we introduce several examples of transition metal oxide [82–86] NWs as electrode materials for pseudo-capacitors.

Among all transition metal oxides, RuO_2 has ultrahigh theoretical SC ($\sim$2000 F/g), excellent electrical conductivity, a wide potential window, long cycle life, and high chemical stability; all of these features have made it one of the most promising candidates for EC electrodes [87–89]. The highest SC value reported was for anodically-deposited amorphous RuO_2 thin films on stainless steel substrates, where a maximum SC of 1190 F/g in H_2SO_4 electrolyte was reported [90]. In comparison, RuO_2 nanorod arrays grown on $LiNbO_3$(100) substrates were reported by Ke et al. [91] to have a SC value of 569 F/g. The decreased SC for the crystalline nanorods versus amorphous films can be attributed to slower transport and diffusion of ions [80, 81]. The major drawbacks of RuO_2 are high cost and toxicity, which prevent it from being used in the commercial ECs. Alternative transition metal oxide materials include MnO_2, NiO, Co_3O_4, and V_2O_5, as well as hybrid mixtures of two or more of these oxides [87–89]. However, these higher abundance and lower toxicity metal oxides have lower conductivity and theoretical SC than RuO_2 [87–89].

For example, Lu et al. [92] reported the synthesis of large-area manganese oxide (MnO_2) nanorod arrays on F-doped SnO_2 (FTO) coated substrates. The free-standing MnO_2 nanorods of 70–100 nm in diameter and 1.5 μm in length were

grown on FTO substrates via anodic electrodeposition in dimethyl sulfoxide (DMSO) aqueous solution. While the theoretical SC is ~1100 F/g [93], electrochemical measurements showed that the MnO_2 nanorod electrodes exhibited SC as high as 660.7 F/g at a scan rate of 10 mV/s and 485.2 F/g at a current density of 3 A/g. Interestingly, during 1500 cycles at room temperature with a current density of 3 A/g, the MnO_2 nanorod electrode SC increased more than 20 % of its initial value over the first 700 cycles, and then retained almost constant SC. This work represents arguably the best reported performance for MnO_2 EC electrodes.

The electrical conductivity of many transition metal oxides is lower than RuO_2, and this limits their SC and power characteristics (due to high charge-transfer resistance). The design of hybrid materials containing different metal oxides, carbon structures, and conductive polymers is a potential route to enhance the electrical conductivity and charge-storage capability by introducing more defects and charge carriers. In addition, coating an ultrathin layer of metal oxide on the surface of a porous, high surface area material can shorten the electron transport distances and thus lead to good electrochemical performance. Xia et al. [94] presented a general two-step solution-based method for the fabrication of transition metal oxide core/shell nanostructure arrays on various conductive substrates. Demonstrated examples include Co_3O_4 on ZnO NW cores and NiO nanoflake shells with a hierarchical and porous morphology (Fig. 8.5a, b). Supercapacitor electrodes based on the Co_3O_4/NiO core/shell NW arrays on a 3D macroporous Ni foam exhibited a high SC of 853 F/g and stable cycling performance up to 6000 cycles (Fig. 8.5c, d).

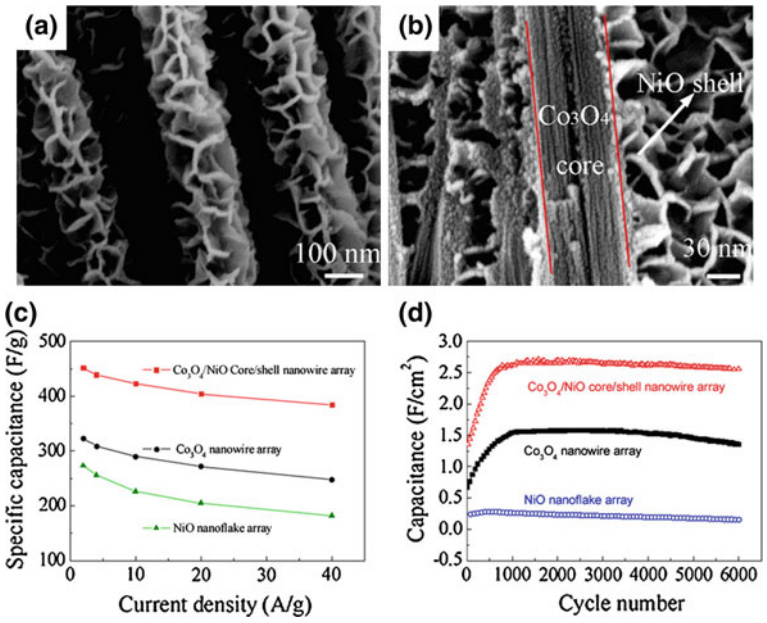

Fig. 8.5 **a**, **b** Co_3O_4/NiO core/shell NW arrays showing the flake morphology of the NiO. **c** SC at different current densities. **d** Cycling performances at 2 A/g. Reproduced from [94]. Copyright 2012 American Chemical Society

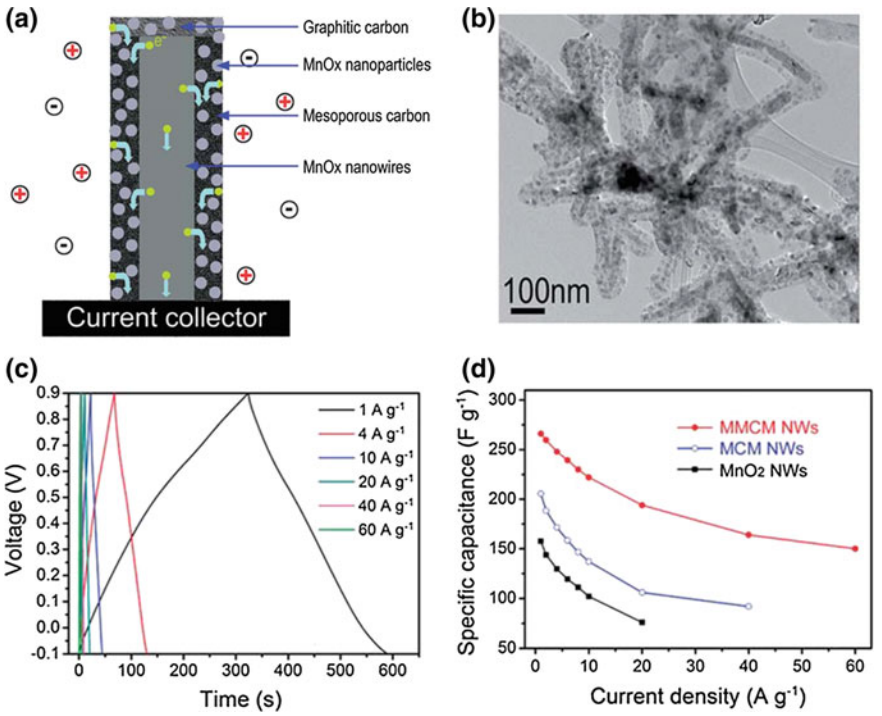

Fig. 8.6 **a**, **b** Schematic and TEM image of the highly graphitic carbon-tipped MMCM hybrid NWs. **c** Charge-discharge curves at 1–60 A g^{-1}. **d** SC as a function of different current densities of the MMCM hybrid NWs (*red lines*), the MCM hybrid NWs (*blue lines*) and the pristine MnO_2 NWs (*black lines*). Reproduced from [97]. Copyright 2011 Royal Society of Chemistry

These results can be compared to the theoretical SC for NiO of 2573 F/g [95]. In 2013, Lou and coworkers [96] developed a cost-effective and simple strategy to design and fabricate novel hierarchical $NiCo_2O_4$@MnO_2 core-shell heterostructured NW arrays on Ni foams for supercapacitor electrodes. These electrodes, which had slim mesoporous $NiCo_2O_4$ NW cores and ultrathin MnO_2 nanoflake shells, achieved a SC value of >1200 F/g.

In addition to those aforementioned hybrid structures, more complex heterostructures have also been demonstrated. For example, Jiang et al. [97] reported the design and synthesis of a highly graphitic carbon-tipped MnO_2/mesoporous carbon/MnO_2 (MMCM) hybrid NW, using a multi-step hydrothermal method combined with soft-template method for mesopore formation (Fig. 8.6a, b). The hybrid NW with optimal carbon content, when applied as an electrode, exhibited superior capacitive properties in 1 M Na_2SO_4 aqueous solution, including high SC of 266 F/g (Fig. 8.6c), rate capability (56.4 % capacity retention at 60 A/g, Fig. 8.6d), and cycling stability without degradation after 1200 cycles. The energy densities achieved was as high as

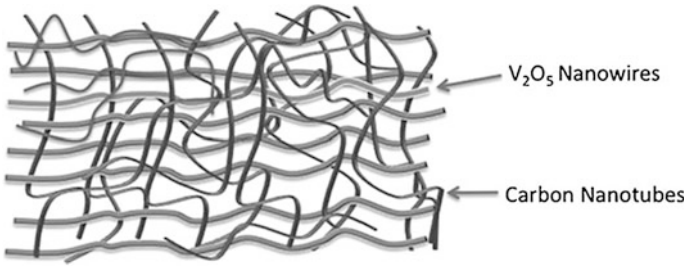

Fig. 8.7 Schematic of method to form supercapacitor material based on interpenetrating networks of CNTs and V_2O_5 NW. Reproduced from [99]. Copyright 2009 John Wiley and Sons

20.8 Wh/kg, at a power density of 30 kW/kg, indicating that the MnO_2 in this hybrid nanomaterial was efficiently utilized with the assistance of the highly conductive graphitic carbon-tipped mesoporous carbon shell.

In addition to hybrid materials containing multiple metal oxides, carbon-based materials have also been extensively used to form hybrid structures with metal oxide NWs for enhancing their electrical conductivity [98]. The Lu group [99] demonstrated the synthesis of hierarchically porous nanocomposites of interpenetrating CNTs and V_2O_5 NW networks (Fig. 8.7), with the SC values of 440 and 200 F/g achieved at current densities of 0.25 and 10 A/g, respectively. In comparison, Boukhalfa et al. [100] used ALD method to deposit ultrathin V_2O_5 on the surfaces of CNTs that were assembled as a self-supporting paper. Flexible electrodes fabricated using this method were able to deliver remarkable SCs of up to 1550 F/g per active mass of the V_2O_5 and 600 F/g per mass of the composite electrode at 1 A/g in 8 M LiCl. Conducting polymers can also applied as the main electrical transport channels for nanocomposites with metal oxides. For instance, Zang et al. [101] demonstrated a one-step in situ co-precipitation approach to synthesize ultrafine MnO_2/polypyrrole (PPy) nanorod composite powders at room temperature. In this approach, pyrrole monomers worked as a reduction agent to reduce Mn^{7+} ions in $KMnO_4$ solution to form Mn^{4+} ions in the form of β-MnO_2 crystal. At the same time the pyrrole monomers were subjected to an oxidative polymerization process to form conductive PPy. The SC of the β-MnO_2 NWs reached as 294 F/g. In another example, Zhou et al. [102] developed a supercapacitor electrode composed of well-aligned CoO NW arrays grown on 3D nickel foam with PPy uniformly immobilized onto or firmly anchored to each NW surface to boost the pseudocapacitive performance. This CoO NW/PPy hybrid electrode reached a SC of 2333 F/g, almost achieving the theoretical value of the hybrid, 2467 F/g.

8.4 Sodium-Ion Batteries

Na-ion batteries (NIBs), as an alternative to LIBs, have attracted extensive investigations, owing to abundant supply and widespread terrestrial reserves of sodium mineral salts [103]. Much progress on developing electrode materials for NIBs has been achieved [103]. Similar to LIB, a NIB consists of two Na intercalation materials as anode and cathode, and share the basic requirements for these electrodes. For instance, single-crystalline layered V_2O_5 NWs were synthesized by a simple solvothermal method, and presented a large (001) interlayer spacing of 11.53 Å, which can accommodate Na ion intercalation [104]. When applied as cathode materials in NIBs, V_2O_5 NWs exhibited a high capacity of 231.4 mAh/g at a current density of 80 mA/g. This capacity corresponds well to the theoretical capacity of 236 mAh/g to form $Na_2V_2O_5$ [105] on Na-ion intercalation. Su et al. [106] demonstrated the synthesis of MnO_2 nanorods with exposed tunnel structures by a hydrothermal method. The as-prepared MnO_2 nanorods had exposed {111} crystal planes, which led to Na ion intercalation/deintercalation, were used as cathode materials for NIBs, with a high initial Na ion storage capacity of 350 mAh/g, and a discharge capacity of 192 mAh/g maintained after 100 cycles, still much lower than the theoretical capacity, 1232 mAh/g [107]. In another report [108], the $Na_4Mn_9O_{18}$ NWs deliver a reversible capacity of 128 mAh/g at 0.1C with an initial capacity retention capability of 77 % after 1000 cycles at 0.5C.

Recently, Kim et al. [109] reported the electrochemical activity of anatase TiO_2 nanorods as anode materials in NIB. The anatase TiO_2 nanorods were synthesized by a hydrothermal method, and their surfaces were coated with carbon to improve the electric conductivity. In cell tests, anodes of bare and carbon-coated anatase TiO_2 nanorods exhibit stable cycling performance and attained a capacity of about 172 and 193 mAh/g on the first charge, respectively, in the voltage range of 3–0 V. The carbon-coated anatase TiO_2 delivered good capacity at high rates, 104 mAh/g at a 10C rate, 82 mAh/g at a 30C rate and 53 mAh/g at a 100C rate, while the theoretical capacity is 1348 mAh/g. In addition, Yuan et al. [110] realized a strategy for fabrication of flexible and porous CuO nanorod arrays by simply engraving commercial copper foils in situ, and the foils were then used directly as the anodes for a NIB. The efficacy of this concept was demonstrated by the high initial capacity of over 640 mAh/g, which is close to the theoretical capacity of 674 mAh/g, for a high charging rate of $\sim$8C at room temperature.

8.5 Future Directions and Challenges

It is important to appreciate the advantages and disadvantages of nanomaterials for electrochemical energy storage, as well as how to control their synthesis and properties [111]. Although NW structures have enabled the potential to provide higher energy density than current energy storage systems, this research field is still

in the developmental stage and will require efforts to understand potentially novel electrochemical behavior in order to achieve practical applications. Specifically, there are challenges facing the development and utilization of NW materials in energy storage, and systematic and detailed studies are still required to promote the progress of this field. For example, further fundamental studies directed toward electrochemical reaction processes and mechanisms in different electrolyte systems (e.g. aprotic, aqueous, hybrid and solid electrolytes) are required to better understand the overall energy storage process. Such studies also will guide the development of novel NW cathode and anode materials, as well as electrolytes and separators.

The research field of NW materials for energy storage has a very bright future, due to the existence of a wide and distinct variety of compounds with various NW structures that have been studied, and will continue to be investigated with foci on discovering new and novel materials, as well as optimizing the performance of the already established ones. As a result, the materials chemistry and electrochemistry of these NW materials will be further enhanced and enriched in the future.

References

1. Y. Demirel, *Energy: Production, Conversion, Storage, Conservation, and Coupling* (Springer, London, 2012)
2. R.H. Crabtree, *Energy Production and Storage: Inorganic Chemical Strategies for a Warming World* (John Wiley & Sons, Chichester, 2010)
3. R.-S. Liu, L. Zhang, X. Sun, H. Liu, J. Zhang, *Electrochemical Technologies for Energy Storage and Conversion* (John Wiley & Sons, Weinheim, 2012)
4. J.Z. Zhang, J. Li, Y. Li, Y. Zhao, *Hydrogen Generation, Storage, and Utilization* (Wiley, Hoboken, New Jersey, 2014)
5. X. Chen, C. Li, M. Grätzel, R. Kostecki, S.S. Mao, Nanomaterials for renewable energy production and storage. Chem. Soc. Rev. **41**(23), 7909–7937 (2012)
6. P.G. Bruce, B. Scrosati, J.M. Tarascon, Nanomaterials for rechargeable lithium batteries. Angew. Chem. Int. Ed. **47**(16), 2930–2946 (2008)
7. C.M. Hayner, X. Zhao, H.H. Kung, Materials for rechargeable lithium-ion batteries. Annu. Rev. Chem. Biomol. Eng. **3**, 445–471 (2012)
8. C.K. Chan, H. Peng, G. Liu, K. McIlwrath, X.F. Zhang, R.A. Huggins, Y. Cui, High-performance lithium battery anodes using silicon nanowires. Nat. Nanotechnol. **3**(1), 31–35 (2008)
9. L. Mai, X. Tian, X. Xu, L. Chang, L. Xu, Nanowire electrodes for electrochemical energy storage devices. Chem. Rev. **114**(23), 11828–11862 (2014)
10. K. Ozawa, *Lithium Ion Rechargeable Batteries: Materials, Technology, and New Applications* (John Wiley & Sons, Weinheim, 2012)
11. G.-A. Nazri, G. Pistoia, *Lithium Batteries: Science and Technology* (Springer, New York, 2008)
12. Y. Wang, G. Cao, Developments in nanostructured cathode materials for high-performance lithium-ion batteries. Adv. Mater. **20**(12), 2251–2269 (2008)
13. H. Wu, Y. Cui, Designing nanostructured Si anodes for high energy lithium ion batteries. Nano Today **7**(5), 414–429 (2012)

14. N.S. Choi, Z. Chen, S.A. Freunberger, X. Ji, Y.K. Sun, K. Amine, G. Yushin, L.F. Nazar, J. Cho, P.G. Bruce, Challenges facing lithium batteries and electrical double-layer capacitors. Angew. Chem. Int. Ed. **51**(40), 9994–10024 (2012)
15. Y. Li, B. Tan, Y. Wu, Mesoporous Co_3O_4 nanowire arrays for lithium ion batteries with high capacity and rate capability. Nano Lett. **8**(1), 265–270 (2008)
16. R.A. Huggins, Lithium alloy negative electrodes. J. Power Sour. **81**, 13–19 (1999)
17. U. Kasavajjula, C. Wang, A.J. Appleby, Nano-and bulk-silicon-based insertion anodes for lithium-ion secondary cells. J. Power Sour. **163**(2), 1003–1039 (2007)
18. K.-Q. Peng, X. Wang, L. Li, Y. Hu, S.-T. Lee, Silicon nanowires for advanced energy conversion and storage. Nano Today **8**(1), 75–97 (2013)
19. X. Su, Q. Wu, J. Li, X. Xiao, A. Lott, W. Lu, B.W. Sheldon, J. Wu, Silicon-based nanomaterials for lithium-ion batteries: a review. Adv. Energy Mater. **4**(1), 1300882 (2014)
20. E. Peled, F. Patolsky, D. Golodnitsky, K. Freedman, G. Davidi, D. Schneier, Tissue-like silicon nanowires-based 3D anodes for high-capacity lithium ion batteries. Nano Lett. **15**(6), 3907–3916 (2015)
21. D.L. Schulz, J. Hoey, J. Smith, A. Elangovan, X. Wu, I. Akhatov, S. Payne, J. Moore, P. Boudjouk, L. Pederson, Si_6H_{12}/polymer inks for electrospinning a-Si nanowire lithium ion battery anodes. Electrochem. Solid-State Lett. **13**(10), A143–A145 (2010)
22. J.Y. Huang, L. Zhong, C.M. Wang, J.P. Sullivan, W. Xu, L.Q. Zhang, S.X. Mao, N.S. Hudak, X.H. Liu, A. Subramanian, In situ observation of the electrochemical lithiation of a single SnO_2 nanowire electrode. Science **330**(6010), 1515–1520 (2010)
23. K. Peng, J. Jie, W. Zhang, S.-T. Lee, Silicon nanowires for rechargeable lithium-ion battery anodes. Appl. Phys. Lett. **93**(3), 033105 (2008)
24. K. Peng, M. Zhang, A. Lu, N.-B. Wong, R. Zhang, S.-T. Lee, Ordered silicon nanowire arrays via nanosphere lithography and metal-induced etching. Appl. Phys. Lett. **90**(16), 163123 (2007)
25. W. Xu, S.S.S. Vegunta, J.C. Flake, Surface-modified silicon nanowire anodes for lithium-ion batteries. J. Power Sour. **196**(20), 8583–8589 (2011)
26. R. Huang, X. Fan, W. Shen, J. Zhu, Carbon-coated silicon nanowire array films for high-performance lithium-ion battery anodes. Appl. Phys. Lett. **95**(13), 133119 (2009)
27. Y. Yao, N. Liu, M.T. McDowell, M. Pasta, Y. Cui, Improving the cycling stability of silicon nanowire anodes with conducting polymer coatings. Energy Environ. Sci. **5**(7), 7927–7930 (2012)
28. C.K. Chan, R.N. Patel, M.J. O'Connell, B.A. Korgel, Y. Cui, Solution-grown silicon nanowires for lithium-ion battery anodes. ACS Nano **4**(3), 1443–1450 (2010)
29. L.-F. Cui, R. Ruffo, C.K. Chan, H. Peng, Y. Cui, Crystalline-amorphous core-shell silicon nanowires for high capacity and high current battery electrodes. Nano Lett. **9**(1), 491–495 (2008)
30. C.K. Chan, R. Ruffo, S.S. Hong, Y. Cui, Surface chemistry and morphology of the solid electrolyte interphase on silicon nanowire lithium-ion battery anodes. J. Power Sour. **189**(2), 1132–1140 (2009)
31. L.-F. Cui, Y. Yang, C.-M. Hsu, Y. Cui, Carbon-silicon core-shell nanowires as high capacity electrode for lithium ion batteries. Nano Lett. **9**(9), 3370–3374 (2009)
32. J. Xie, X. Yang, S. Zhou, D. Wang, Comparing one-and two-dimensional heteronanostructures as silicon-based lithium ion battery anode materials. ACS Nano **5**(11), 9225–9231 (2011)
33. Y. Yao, K. Huo, L. Hu, N. Liu, J.J. Cha, M.T. McDowell, P.K. Chu, Y. Cui, Highly conductive, mechanically robust, and electrochemically inactive TiC/C nanofiber scaffold for high-performance silicon anode batteries. ACS Nano **5**(10), 8346–8351 (2011)
34. K. Evanoff, J. Khan, A.A. Balandin, A. Magasinski, W.J. Ready, T.F. Fuller, G. Yushin, Towards ultrathick battery electrodes: aligned carbon nanotube-enabled architecture. Adv. Mater. **24**(4), 533–537 (2012)

35. X.H. Liu, L.Q. Zhang, L. Zhong, Y. Liu, H. Zheng, J.W. Wang, J.-H. Cho, S.A. Dayeh, S.T. Picraux, J.P. Sullivan, Ultrafast electrochemical lithiation of individual Si nanowire anodes. Nano Lett. **11**(6), 2251–2258 (2011)
36. L. Luo, H. Yang, P. Yan, J.J. Travis, Y. Lee, N. Liu, D. Molina Piper, S.-H. Lee, P. Zhao, S. M. George, Surface-coating regulated lithiation kinetics and degradation in silicon nanowires for lithium ion battery. ACS Nano **9**(5), 5559–5566 (2015)
37. S.W. Lee, M.T. McDowell, J.W. Choi, Y. Cui, Anomalous shape changes of silicon nanopillars by electrochemical lithiation. Nano Lett. **11**(7), 3034–3039 (2011)
38. X.H. Liu, H. Zheng, L. Zhong, S. Huang, K. Karki, L.Q. Zhang, Y. Liu, A. Kushima, W.T. Liang, J.W. Wang, Anisotropic swelling and fracture of silicon nanowires during lithiation. Nano Lett. **11**(8), 3312–3318 (2011)
39. L. Ji, Z. Lin, M. Alcoutlabi, X. Zhang, Recent developments in nanostructured anode materials for rechargeable lithium-ion batteries. Energy Environ. Sci. **4**(8), 2682–2699 (2011)
40. H.B. Wu, J.S. Chen, H.H. Hng, X. Wen Lou, Nanostructured metal oxide-based materials as advanced anodes for lithium-ion batteries. Nanoscale **4**(8), 2526–2542 (2012)
41. J. Jiang, Y. Li, J. Liu, X. Huang, C. Yuan, X.W.D. Lou, Recent advances in metal oxide-based electrode architecture design for electrochemical energy storage. Adv. Mater. **24** (38), 5166–5180 (2012)
42. M. Reddy, G. Subba Rao, B. Chowdari, Metal oxides and oxysalts as anode materials for Li ion batteries. Chem. Rev. **113**(7), 5364–5457 (2013)
43. H. Li, Z. Wang, L. Chen, X. Huang, Research on advanced materials for Li-ion batteries. Adv. Mater. **21**(45), 4593–4607 (2009)
44. A.S. Arico, P. Bruce, B. Scrosati, J.-M. Tarascon, W. Van Schalkwijk, Nanostructured materials for advanced energy conversion and storage devices. Nat. Mater. **4**(5), 366–377 (2005)
45. N. Li, C.J. Patrissi, G. Che, C.R. Martin, Rate capabilities of nanostructured $LiMn_2O_4$ electrodes in aqueous electrolyte. J. Electrochem. Soc. **147**(6), 2044–2049 (2000)
46. A.R. Armstrong, G. Armstrong, J. Canales, R. García, P.G. Bruce, Lithium-ion intercalation into TiO_2-B nanowires. Adv. Mater. **17**(7), 862–865 (2005)
47. M. Saito, Y. Murota, M. Takagi, M. Tajima, T. Asao, H. Inoue, A. Tasaka, M. Inaba, Improvement of the reversible capacity of TiO2 (B) high potential negative electrode. J. Electrochem. Soc. **159**(1), A49–A54 (2011)
48. M.S. Park, G.X. Wang, Y.M. Kang, D. Wexler, S.X. Dou, H.K. Liu, Preparation and electrochemical properties of SnO_2 nanowires for application in lithium-ion batteries. Angew. Chem. **119**(5), 764–767 (2007)
49. D.-W. Kim, I.-S. Hwang, S.J. Kwon, H.-Y. Kang, K.-S. Park, Y.-J. Choi, K.-J. Choi, J.-G. Park, Highly conductive coaxial SnO_2–In_2O_3 heterostructured nanowires for Li ion battery electrodes. Nano Lett. **7**(10), 3041–3045 (2007)
50. H. Kim, J. Cho, Hard templating synthesis of mesoporous and nanowire SnO_2 lithium battery anode materials. J. Mater. Chem. **18**(7), 771–775 (2008)
51. J. Liu, Y. Li, X. Huang, R. Ding, Y. Hu, J. Jiang, L. Liao, Direct growth of SnO_2 nanorod array electrodes for lithium-ion batteries. J. Mater. Chem. **19**(13), 1859–1864 (2009)
52. I.A. Courtney, J. Dahn, Key factors controlling the reversibility of the reaction of lithium with SnO_2 and Sn_2 BPO 6 glass. J. Electrochem. Soc. **144**(9), 2943–2948 (1997)
53. C. Kim, M. Noh, M. Choi, J. Cho, B. Park, Critical size of a nano SnO_2 electrode for Li-secondary battery. Chem. Mat. **17**(12), 3297–3301 (2005)
54. H. Wu, M. Xu, Y. Wang, G. Zheng, Branched Co_3O_4/Fe_2O_3 nanowires as high capacity lithium-ion battery anodes. Nano Res. **6**(3), 167–173 (2013)
55. S. Yang, X. Feng, S. Ivanovici, K. Müllen, Fabrication of graphene-encapsulated oxide nanoparticles: towards high-performance anode materials for lithium storage. Angew. Chem. Int. Ed. **49**(45), 8408–8411 (2010)
56. Y. Wang, G. Cao, Developments in nanostructured cathode materials for high-performance lithium-ion batteries. Adv. Mater. **20**(12), 2251–2269 (2008)

57. J.W. Fergus, Recent developments in cathode materials for lithium ion batteries. J. Power Sour. **195**(4), 939–954 (2010)
58. B.L. Ellis, K.T. Lee, L.F. Nazar, Positive electrode materials for Li-ion and Li-batteries†. Chem. Mat. **22**(3), 691–714 (2010)
59. T. Ohzuku, A. Ueda, Why transition metal (di) oxides are the most attractive materials for batteries. Solid State Ion. **69**(3), 201–211 (1994)
60. F. Jiao, K.M. Shaju, P.G. Bruce, Synthesis of nanowire and mesoporous low-temperature $LiCoO_2$ by a post-templating reaction. Angew. Chem. Int. Ed. **44**(40), 6550–6553 (2005)
61. X. Xiao, L. Yang, H. Zhao, Z. Hu, Y. Li, Facile synthesis of $LiCoO_2$ nanowires with high electrochemical performance. Nano Res. **5**(1), 27–32 (2012)
62. N. Wu, Y. Zhang, Y. Guo, S. Liu, H. Liu, H. Wu, Flake-like LiCoO2 with exposed {010} facets as a stable cathode material for highly reversible lithium storage. ACS Appl. Mater. Interfaces (2016)
63. M. Thackeray, P. Johnson, L. De Picciotto, P. Bruce, J. Goodenough, Electrochemical extraction of lithium from $LiMn_2O_4$. Mater. Res. Bull. **19**(2), 179–187 (1984)
64. Q. Liu, D. Mao, C. Chang, F. Huang, Phase conversion and morphology evolution during hydrothermal preparation of orthorhombic $LiMnO_2$ nanorods for lithium ion battery application. J. Power Sour. **173**(1), 538–544 (2007)
65. M.M. Thackeray, Spinel electrodes for lithium batteries. J. Am. Ceram. Soc. **82**(12), 3347–3354 (1999)
66. D.K. Kim, P. Muralidharan, H.-W. Lee, R. Ruffo, Y. Yang, C.K. Chan, H. Peng, R.A. Huggins, Y. Cui, Spinel $LiMn_2O_4$ nanorods as lithium ion battery cathodes. Nano Lett. **8**(11), 3948–3952 (2008)
67. H.-W. Lee, P. Muralidharan, R. Ruffo, C.M. Mari, Y. Cui, D.K. Kim, Ultrathin spinel $LiMn_2O_4$ nanowires as high power cathode materials for Li-ion batteries. Nano Lett. **10**(10), 3852–3856 (2010)
68. E. Hosono, T. Kudo, I. Honma, H. Matsuda, H. Zhou, Synthesis of single crystalline spinel $LiMn_2O_4$ nanowires for a lithium ion battery with high power density. Nano Lett. **9**(3), 1045–1051 (2009)
69. Y. Wang, Y. Wang, D. Jia, Z. Peng, Y. Xia, G. Zheng, All-nanowire based Li-ion full cells using homologous Mn_2O_3 and $LiMn_2O_4$. Nano Lett. **14**(2), 1080–1084 (2014)
70. M. Freire, N. Kosova, C. Jordy, D. Chateigner, O. Lebedev, A. Maignan, V. Pralong, A new active Li-Mn-O compound for high energy density Li-ion batteries. Nat. Mater. 173–177 (2016)
71. C. Delmas, H. Cognac-Auradou, J. Cocciantelli, M. Menetrier, J. Doumerc, The $Li_xV_2O_5$ system: an overview of the structure modifications induced by the lithium intercalation. Solid State Ion. **69**(3–4), 257–264 (1994)
72. L. Mai, L. Xu, C. Han, X. Xu, Y. Luo, S. Zhao, Y. Zhao, Electrospun ultralong hierarchical vanadium oxide nanowires with high performance for lithium ion batteries. Nano Lett. **10**(11), 4750–4755 (2010)
73. C.K. Chan, H. Peng, R.D. Twesten, K. Jarausch, X.F. Zhang, Y. Cui, Fast, completely reversible Li insertion in vanadium pentoxide nanoribbons. Nano Lett. **7**(2), 490–495 (2007)
74. Q. An, Q. Wei, P. Zhang, J. Sheng, K.M. Hercule, F. Lv, Q. Wang, X. Wei, L. Mai, Three-dimensional interconnected vanadium pentoxide nanonetwork cathode for high-rate long-life lithium batteries. Small **11**(22), 2654–2660 (2015)
75. S. Lim, C.S. Yoon, J. Cho, Synthesis of nanowire and hollow $LiFePO_4$ cathodes for high-performance lithium batteries. Chem. Mat. **20**(14), 4560–4564 (2008)
76. J.R. Miller, P. Simon, Electrochemical capacitors for energy management. Science **321**(5889), 651–652 (2008)
77. P. Simon, Y. Gogotsi, Materials for electrochemical capacitors. Nat. Mater. **7**(11), 845–854 (2008)
78. B.E. Conway, *Electrochemical Supercapacitors: Scientific Fundamentals and Technological Applications* (Springer, New York, 1999)

79. Q. Zhang, E. Uchaker, S.L. Candelaria, G. Cao, Nanomaterials for energy conversion and storage. Chem. Soc. Rev. **42**(7), 3127–3171 (2013)
80. J. Yan, Q. Wang, T. Wei, Z. Fan, Recent advances in design and fabrication of electrochemical supercapacitors with high energy densities. Adv. Energy Mater. **4**(4) (2014)
81. G. Wang, L. Zhang, J. Zhang, A review of electrode materials for electrochemical supercapacitors. Chem. Soc. Rev. **41**(2), 797–828 (2012)
82. X. Wang, X. Wang, W. Huang, P. Sebastian, S. Gamboa, Sol-gel template synthesis of highly ordered MnO_2 nanowire arrays. J. Power Sour. **140**(1), 211–215 (2005)
83. C. Guan, J. Liu, C. Cheng, H. Li, X. Li, W. Zhou, H. Zhang, H.J. Fan, Hybrid structure of cobalt monoxide nanowire @ nickel hydroxidenitrate nanoflake aligned on nickel foam for high-rate supercapacitor. Energy Environ. Sci. **4**(11), 4496–4499 (2011)
84. X.-H. Xia, J.-P. Tu, Y.-J. Mai, X.-L. Wang, C.-D. Gu, X.-B. Zhao, Self-supported hydrothermal synthesized hollow Co_3O_4 nanowire arrays with high supercapacitor capacitance. J. Mater. Chem. **21**(25), 9319–9325 (2011)
85. J. Bae, M.K. Song, Y.J. Park, J.M. Kim, M. Liu, Z.L. Wang, Fiber supercapacitors made of nanowire-fiber hybrid structures for wearable/flexible energy storage. Angew. Chem. Int. Ed. **50**(7), 1683–1687 (2011)
86. P. Yang, Y. Ding, Z. Lin, Z. Chen, Y. Li, P. Qiang, M. Ebrahimi, W. Mai, C.P. Wong, Z.L. Wang, Low-cost high-performance solid-state asymmetric supercapacitors based on MnO_2 nanowires and Fe_2O_3 nanotubes. Nano Lett. **14**(2), 731–736 (2014)
87. J. Zhang, J. Jiang, H. Li, X. Zhao, A high-performance asymmetric supercapacitor fabricated with graphene-based electrodes. Energy Environ. Sci. **4**(10), 4009–4015 (2011)
88. H. Wang, Y. Liang, T. Mirfakhrai, Z. Chen, H.S. Casalongue, H. Dai, Advanced asymmetrical supercapacitors based on graphene hybrid materials. Nano Res. **4**(8), 729–736 (2011)
89. Z.S. Wu, D.W. Wang, W. Ren, J. Zhao, G. Zhou, F. Li, H.M. Cheng, Anchoring hydrous RuO_2 on graphene sheets for high-performance electrochemical capacitors. Adv. Funct. Mater. **20**(20), 3595–3602 (2010)
90. V. Patake, S. Pawar, V. Shinde, T. Gujar, C. Lokhande, The growth mechanism and supercapacitor study of anodically deposited amorphous ruthenium oxide films. Curr. Appl. Phys. **10**(1), 99–103 (2010)
91. Y.-F. Ke, D.-S. Tsai, Y.-S. Huang, Electrochemical capacitors of RuO 2 nanophase grown on $LiNbO_3$ (100) and sapphire (0001) substrates. J. Mater. Chem. **15**(21), 2122–2127 (2005)
92. X. Lu, D. Zheng, T. Zhai, Z. Liu, Y. Huang, S. Xie, Y. Tong, Facile synthesis of large-area manganese oxide nanorod arrays as a high-performance electrochemical supercapacitor. Energy Environ. Sci. **4**(8), 2915–2921 (2011)
93. W. Wei, X. Cui, W. Chen, D.G. Ivey, Manganese oxide-based materials as electrochemical supercapacitor electrodes. Chem. Soc. Rev. **40**(3), 1697–1721 (2011)
94. X. Xia, J. Tu, Y. Zhang, X. Wang, C. Gu, X.-B. Zhao, H.J. Fan, High-quality metal oxide core/shell nanowire arrays on conductive substrates for electrochemical energy storage. ACS Nano **6**(6), 5531–5538 (2012)
95. C. Chen, C. Chen, P. Huang, F. Duan, S. Zhao, P. Li, J. Fan, W. Song, Y. Qin, NiO/nanoporous graphene composites with excellent supercapacitive performance produced by atomic layer deposition. Nanotechnology **25**(50), 504001 (2014)
96. L. Yu, G. Zhang, C. Yuan, X.W.D. Lou, Hierarchical $NiCo_2O_4$@MnO_2 core-shell heterostructured nanowire arrays on Ni foam as high-performance supercapacitor electrodes. Chem. Commun. **49**(2), 137–139 (2013)
97. H. Jiang, L. Yang, C. Li, C. Yan, P.S. Lee, J. Ma, High-rate electrochemical capacitors from highly graphitic carbon-tipped manganese oxide/mesoporous carbon/manganese oxide hybrid nanowires. Energy Environ. Sci. **4**(5), 1813–1819 (2011)
98. P. Chen, H. Chen, J. Qiu, C. Zhou, Inkjet printing of single-walled carbon nanotube/RuO_2 nanowire supercapacitors on cloth fabrics and flexible substrates. Nano Res. **3**(8), 594–603 (2010)

99. Z. Chen, Y. Qin, D. Weng, Q. Xiao, Y. Peng, X. Wang, H. Li, F. Wei, Y. Lu, Design and synthesis of hierarchical nanowire composites for electrochemical energy storage. Adv. Funct. Mater. **19**(21), 3420–3426 (2009)
100. S. Boukhalfa, K. Evanoff, G. Yushin, Atomic layer deposition of vanadium oxide on carbon nanotubes for high-power supercapacitor electrodes. Energy Environ. Sci. **5**(5), 6872–6879 (2012)
101. J. Zang, X. Li, In situ synthesis of ultrafine β-MnO_2/polypyrrole nanorod composites for high-performance supercapacitors. J. Mater. Chem. **21**(29), 10965–10969 (2011)
102. C. Zhou, Y. Zhang, Y. Li, J. Liu, Construction of high-capacitance 3D CoO@polypyrrole nanowire array electrode for aqueous asymmetric supercapacitor. Nano Lett. **13**(5), 2078–2085 (2013)
103. N. Yabuuchi, K. Kubota, M. Dahbi, S. Komaba, Research development on sodium-ion batteries. Chem. Rev. **114**(23), 11636–11682 (2014)
104. D. Su, G. Wang, Single-crystalline bilayered V_2O_5 nanobelts for high-capacity sodium-ion batteries. ACS Nano **7**(12), 11218–11226 (2013)
105. S. Tepavcevic, H. Xiong, V.R. Stamenkovic, X. Zuo, M. Balasubramanian, V.B. Prakapenka, C.S. Johnson, T. Rajh, Nanostructured bilayered vanadium oxide electrodes for rechargeable sodium-ion batteries. ACS Nano **6**(1), 530–538 (2012)
106. D. Su, H.-J. Ahn, G. Wang, β-MnO_2 nanorods with exposed tunnel structures as high-performance cathode materials for sodium-ion batteries. NPG Asia Mater. **5**(11), e70 (2013)
107. L. Feng, Z. Xuan, H. Zhao, Y. Bai, J. Guo, C.-W. Su, X. Chen, MnO_2 prepared by hydrothermal method and electrochemical performance as anode for lithium-ion battery. Nanoscale Res. Lett. **9**(1), 1–8 (2014)
108. Y. Cao, L. Xiao, W. Wang, D. Choi, Z. Nie, J. Yu, L.V. Saraf, Z. Yang, J. Liu, Reversible sodium ion insertion in single crystalline manganese oxide nanowires with long cycle life. Adv. Mater. **23**(28), 3155–3160 (2011)
109. K.-T. Kim, G. Ali, K.Y. Chung, C.S. Yoon, H. Yashiro, Y.-K. Sun, J. Lu, K. Amine, S.-T. Myung, Anatase titania nanorods as an intercalation anode material for rechargeable sodium batteries. Nano Lett. **14**(2), 416–422 (2014)
110. S. Yuan, X.L. Huang, D.L. Ma, H.G. Wang, F.Z. Meng, X.B. Zhang, Engraving copper foil to give large-scale binder-free porous CuO arrays for a high-performance sodium-ion battery anode. Adv. Mater. **26**, 2273–2279 (2014)
111. A.S. Aricò, P. Bruce, B. Scrosati, J.-M. Tarascon, W. Van Schalkwijk, Nanostructured materials for advanced energy conversion and storage devices. Nat. Mater. **4**(5), 366–377 (2005)